Inorg. Chem. **2004**, *43*, 6830–6837

Crystal Structures of $Sr_4Sn_2Se_9$ and $Sr_4Sn_2Se_{10}$ and the Oxidation State of Tin in an Unusual Geometry

Regina Pocha and Dirk Johrendt*

Department Chemie und Biochemie der Ludwig-Maximilians-Universität München, Butenandtstrasse 5-13 (Haus D), 81377 München, Germany

Received March 15, 2004

The new ternary selenostannates $Sr_4Sn_2Se_9$ and $Sr_4Sn_2Se_{10}$ have been synthesized by heating the elements at 1023 K in an argon atmosphere. Their structures were determined by single-crystal X-ray methods. $Sr_4Sn_2Se_9$ crystallizes in a new structure type (*Pbam*, $a = 12.042(2)$ Å, $b = 16.252(3)$ Å, $c = 8.686(2)$ Å, $Z = 4$) with $Sn_2Se_6^{4-}$, $SnSe_4^{4-}$, and Se_2^{2-} subunits. $Sr_4Sn_2Se_{10}$ ($P2_12_12$, $a = 12.028(2)$ Å, $b = 16.541(3)$ Å, $c = 8.611(2)$ Å, $Z = 4$) has a similar structure with Se_3^{2-} triangles instead of Se_2^{2-} dumbbells. Strontium is 8-fold-coordinated by selenium in both cases. The opening angles between tin and the terminal selenium atoms in the Sn_2Se_6 subunits are close to 160°, which is nearer a typical Sn^{2+} coordination geometry than classical $SnSe_4$ tetrahedra. This result suggests the tin oxidation state in the Sn_2Se_6 units to be lower than the expected Sn^{4+}. This question is examined by self-consistent LMTO and LAPW band structure calculations expanded by the Bader analysis of the charge density to assign reliable atomic charges.

Introduction

Within our investigations on ternary and quaternary chalcogenides with complex anions of group 14 elements, we reported recently on the structures and properties of new thiostannates and a selenogermanate with alkaline-earth or europium ions.[1] In general, these solids are built up by either isolated or condensed EQ_4 tetrahedra (E = group 14 element; Q = S, Se), whose terminal chalcogen atoms coordinate the metal ions appropriately. Despite this simple structural motif, the crystal chemistry of thiostannates and their homologues is rich, and numerous crystal structures are known.[2,3] Compounds with alkali metals have been investigated more intensively to study mainly the existence and structures of new complex anions, which are easier to stabilize by soft and polarizable cations.[4] On going to the smaller and higher charged alkaline-earth cations, the ionic contributions to the lattice energy increase by a factor of about 2−3. Thus, the alkaline-earth metals play a more important role for the structure and the physical properties of the materials compared with alkali metals. One subject of our work is to study thiostannates and homologue chalcogenides with group 14 elements of the alkaline-earth metals or europium. Beyond the crystal chemistry we are interested in the physical properties and chemical bonding of these materials.

In this Article, we report on the synthesis and crystal structures of the new selenostannates $Sr_4Sn_2Se_9$ and $Sr_4Sn_2Se_{10}$. Common oxidation states of tin in chalcogenides are 4+ and 2+, but unusual geometries in both compounds suggest a low oxidation state of tin. This interesting problem was recently examined by Gutta and Hoffmann,[5] starting from a molecular mixed-valence tin compound. They suggest that weak secondary interactions may be responsible for the unusual geometries. However, their analysis was made from a somewhat molecular point of view. To shed further light on the question of whether a low-valence tin exists in our selenostannates, we have analyzed the electronic structure and bonding by self-consistent DFT band structure calculations. Since the customary assignment of oxidation states proves to be difficult in the case of our $Sr_4Sn_2Se_9$ and $Sr_4Sn_2Se_{10}$ compounds, we have calculated atomic charges from the topological analysis of the charge density in terms of the atoms-in-molecules (AIM) concept introduced by Bader.

* Author to whom correspondence should be addressed. E-mail: dirk.johrendt@cup.uni-muenchen.de.

(1) Pocha, R.; Tampier, M.; Hoffmann, R.-D.; Mosel, B. D.; Pöttgen, R.; Johrendt, D. *Z. Anorg. Allg. Chem.* **2003**, *629*, 1379.
(2) Olivier-Fourcade, J.; Dumas, J. C.; Ribes, M.; Philippot, E. *J. Solid State Chem.* **1978**, *23*, 155.
(3) Johrendt, D. *Acta Crystallogr.* **2002**, *E58*, i22−i55.
(4) Krebs, B. *Angew. Chem., Int. Ed. Engl.* **1983**, *22*, 13.
(5) Gutta, P.; Hoffmann, R. *Inorg. Chem.* **2003**, *42*, 8161.

10.1021/ic049663y CCC: $27.50
Published on Web 09/24/2004

Table 1. Crystallographic Data for $Sr_4Sn_2Se_9$ and $Sr_4Sn_2Se_{10}$

	$Sr_4Sn_2Se_9$	$Sr_4Sn_2Se_{10}$
fw	5194.00	5509.84
space group	*Pbam* (No. 55)	$P2_12_12$ (No. 18)
a, Å	11.973(2)	12.028(2)
b, Å	16.120(3)	16.541(3)
c, Å	8.594(2)	8.611(2)
V, Å^3	1658.7(3)	1713.2(3)
Z	4	4
temp, K	200(2)	200(2)
λ, Å	0.71073	0.71073
ρ_{calcd}, g·cm^{-3}	5.200	5.340
μ, mm^{-1}	35.45	36.45
Flack parameter		0.60(2)
$R(F)^a$	0.065	0.046
$R_w(F^2)^b$	0.155	0.114

^{a} $R(F) = \sum||F_o| - |F_c||/\sum|F_o|$ for $F_o^2 > 4\sigma(F_o^2)$. ^{b} $R_w(F^2) = [\sum[w(F_o^2 - F_c^2)^2]/\sum w(F_o^2)^2]^{1/2}$ for all data.

Experimental Section

Syntheses. $Sr_4Sn_2Se_9$ and $Sr_4Sn_2Se_{10}$ were synthesized by heating stoichiometric amounts of the elements (all purities > 99.5%) in alumina crucibles, sealed in quartz ampules under atmospheres of purified argon. At first the temperature was raised slowly (50 K h^{-1}) to 1073 K and kept there for 15 h. After cooling, the samples were homogenized in an argon-filled glovebox and heated to 1173 K for 24 h using the same crucibles. This procedure was repeated once more and resulted in homogeneous, dark red powders (almost black), which are not sensitive to air. Small single crystals, suitable for structure determinations, have been selected from the powder samples.

Structure Determinations. X-ray powder patterns of $Sr_4Sn_2Se_9$ and $Sr_4Sn_2Se_{10}$ samples (STOE Stadi-P, Cu Kα_1 radiation, Ge monochromator, 7° PSD detector) could be indexed by using the crystallographic data from the single-crystal experiments. Only small traces of unidentified phases were detected. Single-crystal data were collected on an Enraf-Nonius Kappa CCD diffractometer equipped with a rotating anode. Numerical absorption corrections were performed using the XRED[6] software with crystal faces obtained by the FACEIT[7] system and optimized by XSHAPE.[8] The structures were solved with the direct methods program SHELXS[9] and refined with the full-matrix least-squares program SHELXL.[10] All final refinements included anisotropic displacement parameters. The Flack parameter of $Sr_4Sn_2Se_{10}$ in the noncentrosymmetric space group $P2_12_12$ was 0.60(2), and twin refinements were carried out. Crystal data are reported in Tables 1−5.

Band Structure Calculations. Self-consistent band structure calculations for $Sr_4Sn_2Se_9$ were performed with the linear-muffin-tin-orbital (LMTO) method in its scalar-relativistic version. The TB-LMTO-ASA[11,12] code was used with the crystal orbital Hamilton population (COHP)[13] extension implemented by Boucher.[14] A set of 64 irreducible *k* points were used for reciprocal space integrations by the tetrahedron method. The basis set consisted of Sr 5s/[5p]/4d/[4f], Sn 5s/5p/[5d]/[4f], and Se 4s/4p/[4d] orbitals ("downfolded" orbitals are in brackets). All SCF iterations converged to total energy changes smaller than 10^{-5} Ry.

Two-dimensional grids of the electron localization function (ELF)[15] have been calculated for selected planes in the structure. Regions in space where the Pauli principle does not increase the kinetic energy of the electrons (high values of ELF) can be treated as equivalent to covalent bonds or lone pairs. The COHP method

Table 2. Atomic Coordinates and Equivalent Isotropic Displacement Parameters (pm^2)^a for $Sr_4Sn_2Se_9$

	x	*y*	*z*	U_{eq}
Sr1	0.3868(1)	0.1737(2)	0.2528(2)	148(6)
Sr2	0.2462(2)	0.4280(2)	0.2493(2)	147(6)
Sn1	0.0490(2)	0.1039(2)	0	226(7)
Sn2	0.0899(2)	0.1783(2)	1/2	145(7)
Se1	0.3687(2)	0.3145(2)	0	141(8)
Se2	0	0	0.2269(3)	179(9)
Se3	0.2543(2)	0.0748(2)	0	145(9)
Se4	0.3780(2)	0.3212(2)	1/2	147(9)
Se5	0.2404(2)	0.0697(2)	1/2	146(9)
Se6	0.1308(2)	0.2491(2)	0.2440(2)	182(7)
Se7	0.0414(2)	0.4303(3)	1/2	209(10)
Se8	0.0379(2)	0.4290(3)	0	217(10)

^{a} U_{eq} is defined as one-third of the trace of the orthogonalized U_{ij} tensor.

Table 3. Atomic Coordinates and Equivalent Isotropic Displacement Parameters (pm^2)^a for $Sr_4Sn_2Se_{10}$

	x	*y*	*z*	U_{eq}
Sr1	0.1173(1)	0.6792(1)	0.2417(2)	93(2)
Sr2	0.2541(2)	0.4295(1)	0.2421(2)	102(3)
Sr3	0.3851(1)	0.1786(1)	0.2544(2)	90(3)
Sr4	0.7525(1)	0.0710(1)	0.2591(2)	90(3)
Sn1	0.0528(1)	0.1036(1)	0.4988(2)	174(2)
Sn2	0.0924(1)	0.1739(1)	0.0139(1)	92(2)
Se1	0.0576(1)	0.3912(1)	0.4882(2)	120(3)
Se2	0.1186(1)	0.8253(1)	0.0051(1)	89(2)
Se3	0.1303(2)	0.2387(1)	0.2773(2)	123(3)
Se4	0.2453(1)	0.0696(1)	0.0118(2)	88(2)
Se5	0.2578(1)	0.0730(1)	0.5127(2)	82(2)
Se6	0.3715(1)	0.3183(1)	0.4952(2)	85(2)
Se7	0.5606(1)	0.1070(1)	0.0108(2)	130(2)
Se8	0.6328(2)	0.2518(1)	0.2351(1)	109(3)
Se9	0	1/2	0.1576(2)	122(3)
Se10	0	1/2	0.6515(2)	111(3)
Se11	0	0	0.2780(2)	106(4)
Se12	0	0	0.7256(2)	123(4)

^{a} U_{eq} is defined as one-third of the trace of the orthogonalized U_{ij} tensor.

Table 4. Selected Bond Lengths (Å) and Angles (deg) for $Sr_4Sn_2Se_9$

Sr1−Se1	3.150(3)	Sn2−Se6 (2×)	2.526(2)
Sr1−Se3	3.127(3)	Sn2−Se4	2.538(3)
Sr1−Se5	3.244(3)	Se7−Se7	2.458(8)
Sr1−Se4	3.189(3)	Se8−Se8	2.461(8)
Sr1−Se6	3.177(3)	Sr2−Se1	3.176(3)
Sr1−Se6	3.298(3)	Sr2−Se2	3.259(2)
Sr1−Se7	3.278(3)	Sr2−Se3	3.191(4)
Sr1−Se8	3.244(3)	Sr2−Se4	3.178(3)
Sn1−Se3	2.503(3)	Sr2−Se5	3.144(4)
Sn1−Se1	2.528(4)	Sr2−Se6	3.198(3)
Sn1−Se2 (2×)	2.636(3)	Sr2−Se7	3.264(3)
Sn1−Se6 (2×)	3.359(3)	Sr2−Se8	3.288(3)
Sn2−Se5	2.512(4)		

Se1−Sn1−Se3	159.5(2)	Se6−Sn2−Se5 (2×)	100.1(1)
Se2−Sn1−Se3 (2×)	95.7(1)	Se6−Sn2−Se6	121.1(2)
Se2−Sn1−Se1 (2×)	98.1(1)	Se4−Sn2−Se5	136.0(2)
Se2−Sn1−Se2	95.4(1)	Se4−Sn2−Se6 (2×)	101.1(1)

(6) X-RED data reduction, Rev. 1.19, Stoe & Cie GmbH, 1999.
(7) FACEIT Video System, Stoe & Cie GmbH, 1998.
(8) X-SHAPE, Crystal optimization for numerical absorption correction, Rev. 1.06, Stoe & Cie GmbH, 1999.
(9) Sheldrick, G. M. SHELXS-A program for crystal structure solution, Universität Göttingen, 1997.
(10) Sheldrick, G. M. SHELXL-A program for crystal structure refinement, Universität Göttingen, 1997.
(11) Andersen, O. K.; Jepsen, O. Tight-Binding LMTO Vers. 47c, Max-Planck-Institut für Festkörperforschung, Stuttgart, 1994.
(12) Skriver, H. L. *The LMTO method: muffin-tin orbitals and electronic structure*; Springer-Verlag: Berlin, New York 1984.
(13) Dronskowski, R.; Bloechl, P. E. *J. Phys. Chem.* **1993**, *97* (33), 8617.
(14) Boucher, F.; Rousseau, R. *Inorg. Chem.* **1998**, *37* (10), 2351.
(15) Savin, A.; Silvi, B. *Nature* **1994**, *371*, 683.

Table 5. Selected Bond Lengths (Å) and Angles (deg) for $Sr_4Sn_2Se_{10}$

Sr1−Se5	3.136(2)	Sn2−Se8	2.519(2)
Sr1−Se2	3.160(2)	Sn2−Se4	2.520(2)
Sr1−Se1	3.207(2)	Sn2−Se2	2.539(2)
Sr1−Se8	3.216(2)	Sn2−Se3	2.550(2)
Sr1−Se6	3.232(2)	Se9−Se7 (2×)	2.401(2)
Sr1−Se7	3.276(2)	Se10−Se1 (2×)	2.387(2)
Sr1−Se4	3.284(2)	Sr3−Se6	3.109(2)
Sr1−Se3	3.287(2)	Sr3−Se7	3.203(2)
Sr2−Se2	3.139(2)	Sr3−Se5	3.217(2)
Sr2−Se5	3.179(2)	Sr3−Se8	3.220(2)
Sr2−Se6	3.182(2)	Sr3−Se3	3.228(2)
Sr2−Se4	3.186(2)	Sr3−Se4	3.232(2)
Sr2−Se12	3.191(2)	Sr3−Se1	3.248(2)
Sr2−Se1	3.237(2)	Sr3−Se2	3.298(2)
Sr2−Se7	3.245(2)	Sr4−Se6	3.142(2)
Sr2−Se9	3.352(2)	Sr4−Se4	3.154(2)
Sn1−Se5	2.520(1)	Sr4−Se2	3.183(2)
Sn1−Se6	2.535(1)	Sr4−Se7	3.202(2)
Sn1−Se11	2.637(2)	Sr4−Se11	3.205(2)
Sn1−Se12	2.675(2)	Sr4−Se5	3.234(2)
Sn1−Se3	3.082(2)	Sr4−Se1	3.259(2)
Sn1−Se8	3.449(2)	Sr4−Se8	3.326(2)
Se5−Sn1−Se6	160.6(1)	Se2−Sn2−Se8	99.5(1)
Se5−Sn1−Se11	98.02(4)	Se2−Sn2−Se4	137.1(1)
Se6−Sn1−Se11	97.96(4)	Se3−Sn2−Se8	121.2(1)
Se5−Sn1−Se12	93.93(4)	Se3−Sn2−Se4	99.5(1)
Se6−Sn1−Se12	96.14(4)	Se3−Sn2−Se2	101.7(1)
Se11−Sn1−Se12	93.03(5)	Se7−Se9−Se7	105.7(1)
Se4−Sn2−Se8	100.8(1)	Se1−Se10−Se1	107.8(1)

was used for the bond analysis. COHP gives the energy contributions of all electronic states for a selected bond. Since the values are negative for bonding states, we plot −COHP(E) to get positive values according to the well-known COOP diagrams.

Topologies of interatomic surfaces[16,17] were calculated from the charge density distribution $\rho(r)$ obtained by DFT-based calculations with the WIEN2k program package[18,19] using the FP-LAPW method within the GGA approximation. The total energies and charge densities of the preceding SCF cycles converged to changes smaller than 10^{-4}. The basis set consisted of 955 plane waves up to a cutoff $R_{mt}K_{max} = 7$. The atomic sphere radii R_{mt} were 2.6, 2.3, and 2.2 au for Sr, Sn, and Se, respectively. A total of 30 k points were used in the irreducible wedge of the Brillouin zone. To get a good charge density for the Bader analysis, we used *LM* values for the lattice harmonics expansion[20] up to $L = 9$ for all atoms. Atomic charges were assigned by integrations of the charge density within the interatomic surfaces (IASs) (which is the zero-flux surface of ρ, where $\nabla\rho\cdot\mathbf{n} = 0$ holds), and subtracting the nuclear charge of the corresponding atom.

Results

Crystal Structures. As seen from Figure 1, both ternary compounds form similar orthorhombic structures with four $SnSe_4^{4-}$ and two $Sn_2Se_6^{4-}$ selenostannate subunits per unit cell. $Sr_4Sn_2Se_9$ contains moreover four Se_2^{2-} diselenide and $Sr_4Sn_2Se_{10}$ four Se_3^{2-} triselenide groups with Se−Se distances of 2.401−2.461 Å and angles Se−Se−Se of 105.7(1)° and 107.8(1)°, respectively. This leads to the formulas $Sr_8(Sn_2Se_6)(SnSe_4)_2(Se_2)_2$ and $Sr_8(Sn_2Se_6)(SnSe_4)_2(Se_3)_2$, and the full names of these compounds are strontium diselenostannate selenostannate diselenide and strontium diselenostannate selenostannate triselenide, respectively. The structure of $Sr_4Sn_2Se_{10}$ is isotypic to that of $Eu_8(Sn_4Se_{14})(Se_3)_2$ reported by Evenson and Dorhout.[21] The latter compound was already mentioned as "Eu_2SnSe_5" by Flahaut et al.,[22] who assigned the structure mistakenly to the La_2SnS_5 type[23] with trivalent europium. The same authors implied also the existence of the corresponding strontium compounds, but structural data were not reported.

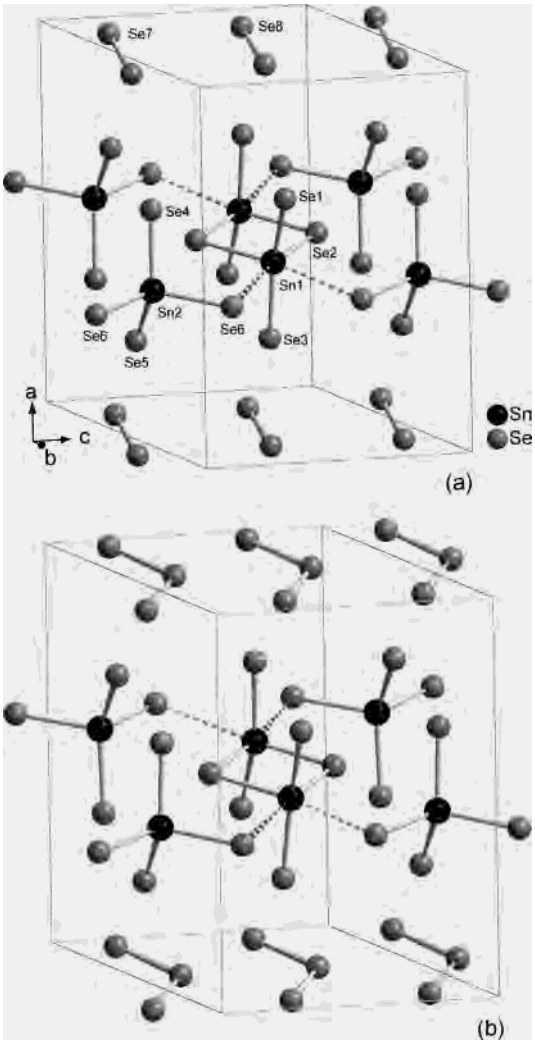

Figure 1. Covalently bonded $Sn_2Se_6^{4-}$, $SnSe_4^{4-}$, Se_2^{2-}, and Se_3^{2-} subunits in the unit cells of $Sr_4Sn_2Se_9$ (a) and $Sr_4Sn_2Se_{10}$ (b). All strontium atoms and the second $Sn_2Se_6^{4-}$ group in the cell are not shown for clarity.

Figure 1 emphasizes the arrangements of the covalently bonded subunits in the unit cells of $Sr_4Sn_2Se_9$ (a) and $Sr_4Sn_2Se_{10}$ (b). Tin is 4-fold-coordinated by selenium atoms in the first coordination sphere, and the Sn−Se bond lengths vary between 2.503 and 2.675 Å, which is in the range of the sum of the covalent radii for tin and selenium of 2.57 Å.

(16) Bader, R. F. W. *Atoms in molecules—a quantum theory*; Clarendon Press: Oxford, 1994.
(17) Popelier, P. *Atoms in molecules—an introduction*; Pearson Education Ltd.: Vienna, Austria, 2000.
(18) Blaha, P.; Schwarz, K.; Madsen, G. K. H.; Kvasnicka, D.; Luitz, J. WIEN2k-An Augmented Plane Wave + Local Orbitals Program for Calculating Crystal Properties, TU Wien, 2001.
(19) Schwarz, K.; Blaha, P. *Comput. Mater. Sci.* **2003**, *28*, 259.
(20) Kara, M.; Kurki-Suonio, K. *Acta Crystallogr.* **1981**, *A37*, 201.
(21) Evenson IV, C. R.; Dorhout, P. K. *Z. Anorg. Allg. Chem.* **2001**, *627*, 2178.
(22) Flahaut, J.; Laruelle, P.; Guittard, M.; Jaulmes, S.; Pouzol, M. J.; Lavenent, C. *J. Solid State Chem.* **1979**, *29*, 125.
(23) Jaulmes, S. *Acta Crystallogr.* **1974**, *B30*, 2283.

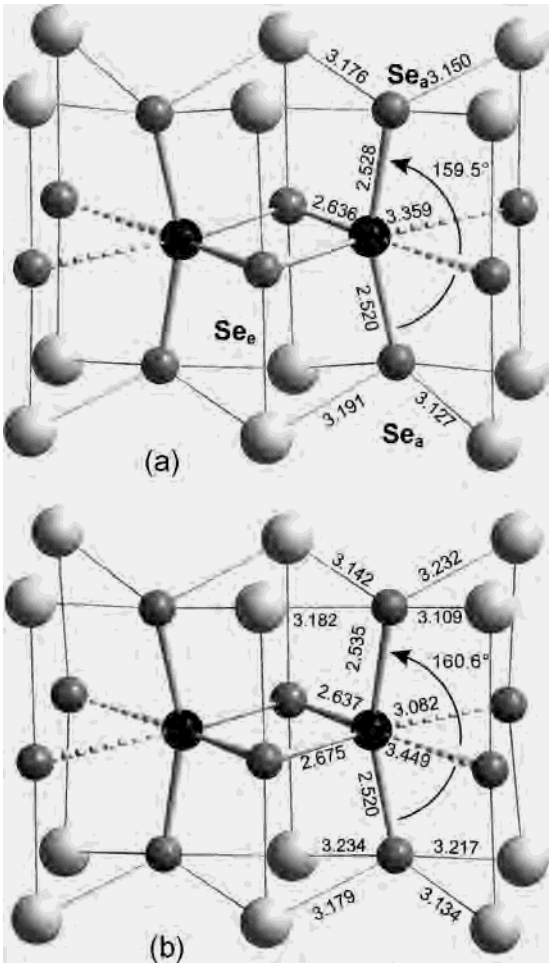

Figure 2. Coordination geometries of the Sn_2Se_6 subunits in (a) $Sr_4Sn_2Se_9$ and (b) $Sr_4Sn_2Se_{10}$ (black spheres, Sn; gray spheres, Se; light gray spheres, Sr; all distances in angstroms).

The dotted lines indicate possible weak secondary interactions with a Sn···Se distance of 3.359 Å in $Sr_4Sn_2Se_9$, which splits to 3.082 and 3.449 Å in $Sr_4Sn_2Se_{10}$. Thus, all important Sn−Se bond lengths and angles are as expected for typical Sn^{4+}−Se bonds in $SnSe_4$ tetrahedra. This does not hold true for the Se−Sn−Se bond angle between tin and the axial (Se_a) atoms of the Sn_2Se_6 groups (Se1 and Se3 in Figure 1a), which is 159.5(2)° in $Sr_4Sn_2Se_9$ and 160.6(1)° in $Sr_4Sn_2Se_{10}$. Figure 2 shows detailed geometries around the tin atoms in the Sn_2Se_6 groups, together with the neighboring Sr atoms. In both cases, the Se_a−Sn−Se_a bond angles are ∼46% larger compared to the tetrahedral angle (109.47°), but differ from a linear coordination by only ∼11%. At first sight, the coordination around the Sn atoms in Figure 2 looks like a distorted octahedron. But the question arises of whether we have to consider the two selenium atoms at ∼3.36 Å as (weakly) bonded to tin. First, in usual $Sn_2Se_6^{4-}$ units as found, for example, in $Cs_4Sn_2Se_6$,[24] we have Sn^{4+}−Se distances of 2.47−2.65 Å and axial angles of ∼116°, as expected for tetrahedrally bonded Sn^{4+}. From the literature data we find that selenostannates never form Sn^{4+}−Se bonds longer than ∼2.85 Å, not even in the case of 5-fold coordination. Longer Sn−Se distances are exclusively observed in true Sn^{2+} compounds, for example, in orthorhombic SnSe (3.46 Å)[25] or the mixed-valence compound $K_2Sn_4Se_8$ (3.13 Å).[26] Nevertheless, we can assume some electrostatic interaction between the tin atoms in our Sn_2Se_6 units and the Se6 atoms, and one may argue whether this could be a reason for the opening of the axial angle. However, comparable selenostannates with such a 4(+2) coordination are not known, but at least one additional selenium coming from the equatorial direction obviously causes no large Se_a−Sn−Se_a angles. This becomes evident from the structure of $K_2Sn_2Se_5$,[27] shown in Figure 3. Tin is 5-fold-coordinated with Sn^{4+}−Se bond lengths of 2.510−2.857 Å. Although the "$Sn_2Se_4Se_{4/2}$" subunits in $K_2Sn_2Se_5$ are connected, the structure could easily open the angle by changing the position of the terminal Se atom. But the angle of concern is still 124.97°, as depicted in Figure 3. Thus, the long Sn···Se bond between our $Sn_2Se_6^{4-}$ and $SnSe_4^{4-}$ units is probably not the reason for the geometry of our $Sn_2Se_6^{4-}$ subunits.

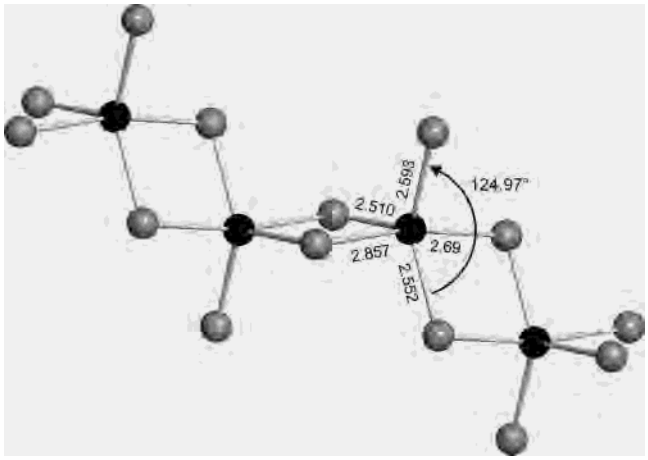

Figure 3. Part of the $K_2Sn_2Se_5$ structure with tin in 5-fold coordination.

Nevertheless, such wide angles suggest the oxidation state of this tin site to be lower than Sn^{4+}, because this geometry is reminiscent of typical Sn^{2+} compounds with a lone pair as the fifth ligand. This has been found in $K_2Sn_4Se_8$, which contains besides $Sn^{4+}Se_4$ tetrahedra also one Sn^{2+} site with a pseudo-bipyramidal coordination of four seleniums and the tin lone pair. The axial Se_a−Sn−Se_a angle is 177°, but the more important fact is that the Sn^{2+}−Se_a distances in $K_2Sn_4Se_8$ are 3.132 Å, as typical and expected for Sn^{2+}. In contrast to this, all axial and equatorial Sn−Se bonds in the Sn_2Se_6 subunits of $Sr_4Sn_2Se_9$ are around 2.6 Å. From this we can rule out the presence of pure Sn^{2+} and $Sn_2Se_6^{6-}$ groups. Consequently, the long Sn···Se contacts probably play no decisive role if the tin atoms are Sn^{4+}. But the question of an intermediate oxidation state such as Sn^{3+} remains open. In their recently published paper, Gutta and Hoffmann[5] pursued just this question of a potential Sn^{3+} chemistry in our compounds. The authors used DFT calculations on different molecular models of $Sn_2Se_6^{n-}$, a set of extended Hückel band structure calculations, and detailed MO considerations, but all methods did not yield a conclusive answer.

(24) Sheldrick, W. S.; Braunbeck, H. G. *Z. Naturforsch.* **1988**, *44b*, 851.
(25) Wiedemeyer, H.; von Schnering, H. G. *Z. Kristallogr.* **1978**, *148*, 295.
(26) Klepp, K. O.; Fabian, F. *Z. Naturforsch.* **1992**, *47b*, 406.
(27) Klepp, K. O. *Z. Naturforsch.* **1992**, *47b*, 197.

In the end, they suggested a normal Sn^{4+} may still be an appropriate description. They also suspect that the above-mentioned secondary interactions may be responsible for the unusual geometry. But according to our argumentation, these two results exclude each other, because such long Sn···Se bonds are reasonable only with Sn^{2+}. We will come back to this question later on. Before we do this, we want to emphasize another important part of our structures, namely, the Sr^{2+} ions, which surround all selenium atoms of the $Sn_2Se_6^{4-}$ and $SnSe_4^{4-}$ subunits. As seen from Figure 2, the axial Se_a atoms are bonded to four Sr atoms. Any decrease of the $Se_a-Sn-Se_a$ angle must alter the Sr−Se contacts dramatically and would require a rearrangement of the structure. We think that the energy for such a structural reorganization is probably much larger than the energy loss by opening the $Se_a-Sn-Se_a$ angle from 109.47° to 160.6(1)°. However, this cannot be proved here. But it seems the more probable explanation, if no other conclusive proof can be derived from the electronic structure.

Figure 4 emphasizes the coordination polyhedra of the strontium atoms in the crystal structure of $Sr_4Sn_2Se_9$ and $Sr_4Sn_2Se_{10}$. Eight selenium atoms coordinate the strontium atoms in a bicapped trigonal prismatic arrangement, and the Sr−Se distances are 3.156−3.322 Å. Each $SrSe_8$ prism has four face-, one edge-, and two corner-sharing neighbors. This dense three-dimensional polyhedral linkage leaves square and rhombic channels along [001]. The square channels are filled with the Sn atoms, and the short diameters of the rhombic channels represent the short Se−Se distances of the diselenide units or contain the central Se atom of the triselenide groups in the case of $Sr_4Sn_2Se_{10}$.

Chemists tend to find molecules in solid-state compounds by classifying bonding interactions. This is often appropriate and meaningful, but one must be aware of favoring covalent interactions (chemists like them most) over all other contributions, especially in close-packed and substantially ionic solids. In our case, the tin−selenium and Se_2/Se_3 subunits are the covalently bonded "molecular" entities in $Sr_4Sn_2Se_9$ and $Sr_4Sn_2Se_{10}$. But there are 3 times more Sr−Se than Sn−Se bonds (24:8) in our structures, and for that reason alone the electrostatic forces between the Sr^{2+} and the $Se^{2-(1-)}$ ions contribute main parts to the bonding energy. Therefore, it is in our opinion not reasonable to assume that the geometries of the $SnSe_4$ and Sn_2Se_6 subunits are independent from the coordination of the strontium ions. It is worthwhile to note that we have a comparable situation in Eu_2SnS_4.[1] The thiostannate tetrahedra are likewise distorted (S−Sn−S angles up to 136°), and the tin atoms are also in square channels within a network of comparable EuS_7 polyhedra. These similarities support the idea that one reason for the unusual bond angles in $Sn_2Se_6^{4-}$ may be the optimal coordination of the Sr ions rather than a question of the oxidation state of tin or weak secondary interactions.

So far it seems probable that the driving force for the large $Se_a-Sn-Se_a$ angle in the Sn_2Se_6 subunits is no electronic effect coming from the "molecule" itself. But nevertheless the resulting geometry *favors* a lower oxidation state in terms of a higher electronic population of the tin atoms. This, however, raises the question of whether in the structure there exists any atom or group which could be able to provide electrons for (at least) a partial reduction of tin. To shed light on this and other questions of chemical bonding in $Sr_4Sn_2Se_9$, we have performed self-consistent DFT band structure calculations.

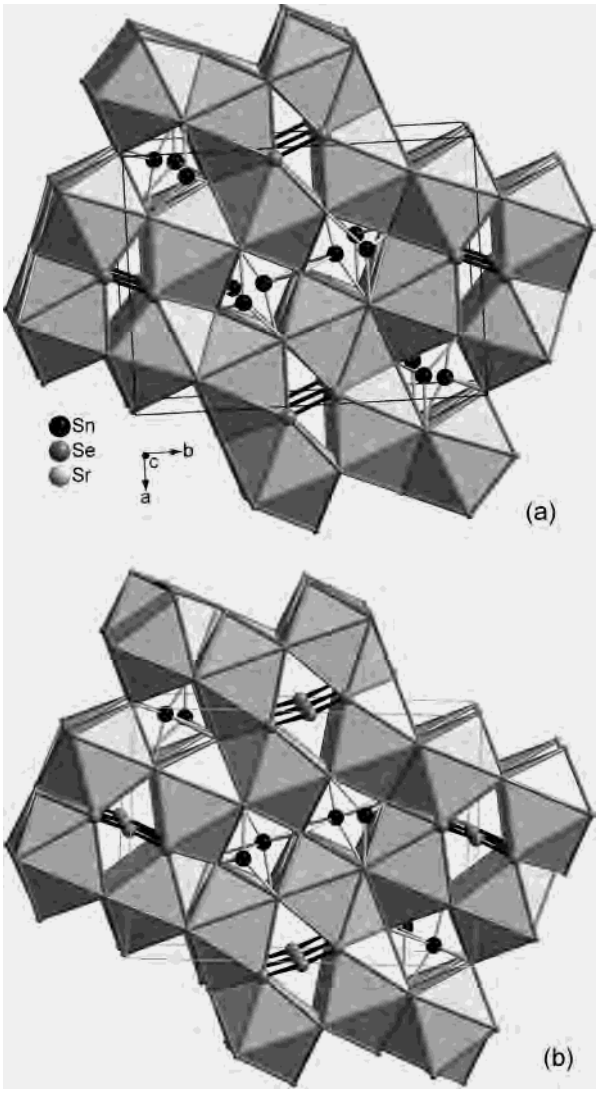

Figure 4. Crystal structures of $Sr_4Sn_2Se_9$ (a) and $Sr_4Sn_2Se_{10}$ (b). The coordination polyhedra of strontium are emphasized. All tin atoms are in square channels running along [001]. Thick black lines represent the bonds of the Se_2 and Se_3 groups, respectively.

Electronic Structure, Chemical Bonding, and Electronic Populations. The main features of the electronic band structures of $Sr_4Sn_2Se_9$ and $Sr_4Sn_2Se_{10}$ are very similar; therefore, we confine our discussion to the centrosymmetric compound $Sr_4Sn_2Se_9$. The total density of states (DOS) and selected DOS projections are shown in Figure 5. A gap is discerned at the Fermi level, as expected from the ionic formula splitting $(Sr^{2+})_4(Sn^{4+})_2(Se^{2-})_7(Se_2)^{2-}$. $Sr_4Sn_2Se_9$ is a semiconductor with a calculated energy gap of ∼0.8 eV. This value is underestimated by the LDA, but a gap smaller than 1.5 eV is consistent with the deep red, almost black color of the compound. The valence band between −4 eV and the Fermi level consists mainly of the Sn−Se bonding Se 4p states and also a significant contribution of Sr 4d states.

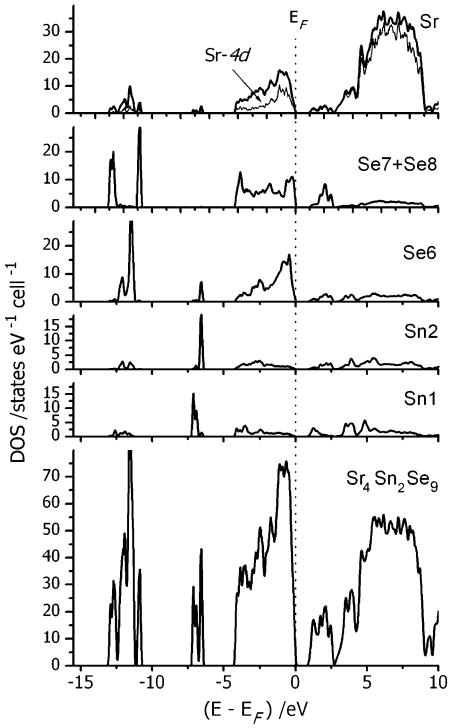

Figure 5. Total and partial DOS of $Sr_4Sn_2Se_9$. The energy zero is taken at the Fermi level.

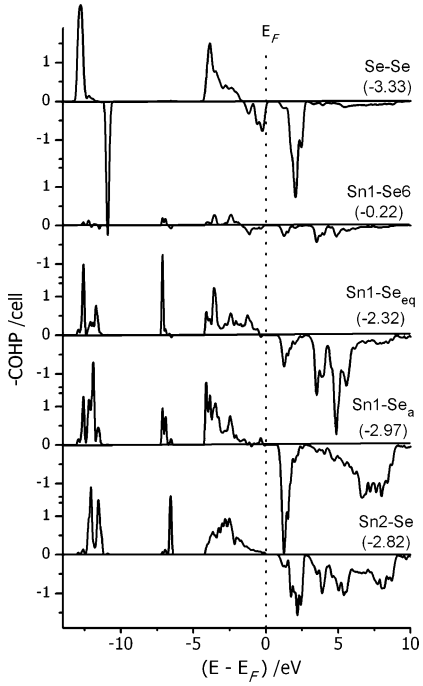

Figure 6. COHP diagrams of selected bonds in $Sr_4Sn_2Se_9$. Numbers in parentheses are ICOHP values in electronvolts per bond (COHP integration up to E_F).

The latter already implies that the real charge of the strontium atoms is lower than the formal 2+. However, the DOS does not permit the calculation of reliable values for atomic charges, because from DOS integrations one gets merely the amount of charge inside the atomic spheres. The lowest part of the conduction band between E_F and ~2.5 eV is interestingly enough dominated by the Sn 5s and the Se 4p states from the Se_2 subunits (Se7/Se8) and the Se6 atoms.

Figure 6 shows the bonding features of selected pairs. As expected, all Sn−Se bonding states of the $Sn1_2Se_6^{4-}$ and $Sn2Se_4^{4-}$ subunits are occupied and well below the Fermi level. Their ICOHP bond energies are −2.32 to −2.97 eV/bond, as marked in Figure 6. The energy values for the short Sn−Se bonds scale approximately with the distances, while the computed ICOHP of −0.22 eV for the Sn1···Se6 interaction is 1 order of magnitude smaller. It is known for the COHP method that such small values are not reliable due to (small) dependencies of the Hamiltonian on the ASA sphere radii.[28] Thus, we cannot decide from the COHP picture whether we have significant bonding between the tin atoms of $Sn1_2Se_6^{4-}$ and the Se6 atoms of the neighboring $Sn2Se_4^{4-}$. But it is clear that, if any Sn1···Se6 bonding is present, it is very weak. On the other hand, the bond angle deviation of more than 45° is certainly very large. Thus, in our opinion, the COHP results permit no conclusion regarding the wide Se_a−Sn1−Se_a angle.

Nonetheless, the COHP reveals a plausible mechanism to reduce the tin atoms. The lowest lying Sn−Se antibonding states of the conduction band are from the axial Sn1−Se_a bonds of the $Sn_2Se_6^{4-}$ groups with strong Sn 5s character. At the same time, we see the antibonding π^* orbitals of the Se_2^{2-} subunits occupied in the vicinity of the Fermi level. One might speculate that any oxidation of Se_2^{2-} would transfer electrons to reduce the oxidation state of Sn1 atoms. This should result in stronger and shorter Se−Se bonds. But, as already shown by Gutta and Hoffmann,[5] there is no indication toward shorter Se−Se bonds in Se_2^{2-} or Se_3^{2-}, so this mechanism cannot be proved.

The ELF can be a suitable tool to track a lower valence state of the tin atoms in the $Sn_2Se_6^{4-}$ units by uncovering lone pairs. Figure 7a shows the contour diagram of the ELF topology in the equatorial plane of $Sr_4Sn_2Se_9$, showing the Sn1−Se_{eq} bonds in Sn_2Se_6 and the Sn_2−Se_6 bonds of the $SnSe_4$ units. The short covalent Sn−Se bonds are clearly visible and have similar ELF topologies. We see no indication for a Sn1···Se6 bond in the ELF. Figure 7b depicts the axial plane of the Sn_2Se_6 subunit with the Se_a−Sn1−Se_a bonds. Within the Sn_2Se_6 group, we discern high ELF values in the bonding region between Sn and Se_a and also the lone pairs at Se. This picture is not much different from that of a normal tetrahedral $Sn^{4+}Se_4$ group shown in Figure 7a. We have also calculated the ELF within the axial plane of the trigonal-bipyramidal $Sn^{2+}Se_4$ unit in $K_2Sn_4Se_8$, shown in Figure 7c. The differences between tin in Sn_2Se_6 and the true Sn^{2+} are evident. We discern the distinctive lone pair at the tin site. More important, we see no localization between the tin and selenium nuclei, which means that the Sn^{2+}−Se bonds are considerably more ionic (and longer) than the tetrahedral Sn^{4+}−Se bonds. Thus, from the ELF topology we receive also no hint for a low oxidation state of tin in the Sn_2Se_6 subunits of $Sr_4Sn_2Se_9$.

Although all results so far point clearly toward Sn^{4+} in our compounds, it is clear that the almost linear Se_a−Sn−

(28) Boucher, F. Institut des Materiaux de Nantes, IMN-CMRS, Nantes, France, Private communication, 1999.

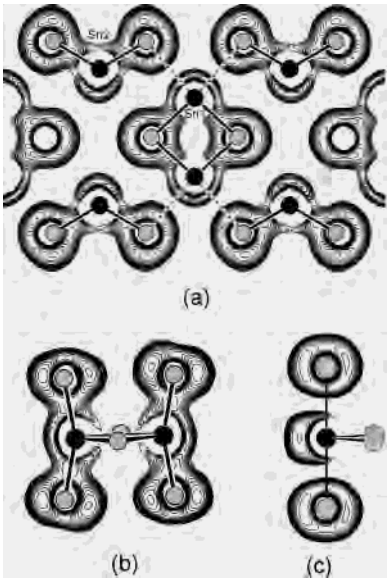

Figure 7. Contours of the electron localization function (ELF = 0.6−0.92) in $Sr_4Sn_2Se_9$: (a) equatorial plane of the Sn_2Se_6 subunit with the Sn1−Se_{eq} bonds (dotted lines indicate the Sn1−Se6 interactions) and the Sn2−Se6 bonds of the $SnSe_4$ tetrahedra; (b) axial plane of the Sn_2Se_6 subunit with the Sn1−Se_a bonds; (c) axial plane of the pseudo-bipyramidal Sn^{2+}-Se_4 in $K_2Sn_4Se_8$.

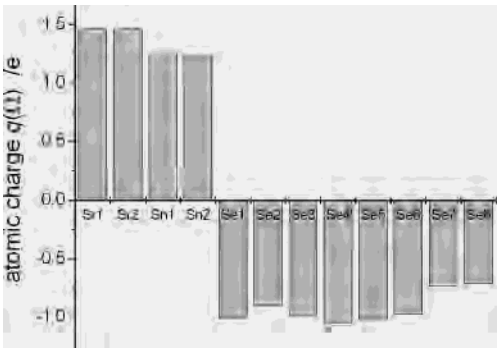

Figure 8. AIM charges of the atom sites in $Sr_4Sn_2Se_9$ obtained by integration of $\rho(r)$ in the atomic basins Ω.

Se_a geometry still favors an accumulation of electrons in a more or less distinct lone pair at the tin site. Thus, the chemist's useful concept of assigning oxidation states by considering electronegativities and electron counts is obviously inconsistent with the observed geometry. We can consider the present case as a typical example for the weakness of the term "oxidation state", whose definition is not very precise. Instead of this we can ask for the atom's electronic population $N(\Omega) = \int_\Omega \rho(r)\, d\tau$ within the atomic basin Ω, i.e., the amount of charge in the portion of space the atom occupies. Within AIM theory, the boundaries of the atomic basins are defined by the IASs. The IAS or zero flux surface is a topological manifold constructed from a bundle of gradient paths of the electron density $\rho(r)$. The atomic charge of an atom A is then defined as $q_A = N_A - Z_A$. Figure 8 shows the result of the charge integrations for all unique atom positions in $Sr_4Sn_2Se_9$. The sum of charges in all atomic basins of the unit cell is 0.0067e, and we estimate an error of ±0.01e for each value, keeping in mind that absolute values of equal atom types at different crystallographic positions may vary easily by ±0.1 due to different spatial environments. The strontium atoms show the highest cation charge of $q_{Sr} = +1.46$, almost equal at both Sr sites as expected from the identical coordination. But in contrast to this, we find also the same charges for the tin atoms in $SnSe_4$ with $q_{Sn2} = +1.23$ and in the Sn_2Se_6 subunits with $q_{Sn1} = +1.25$ *despite* their very different geometries. The charges of the selenium atoms are −0.71 in the Se_2 dumbbells and −0.89 for the bridging Se2 in Sn_2Se_9 and range from −0.97 to −1.04 for all terminally bonded Se. These results reflect the trend expected from the chemist's oxidation numbers (Sr^{2+}, Sn^{4+}, Se^{2-}, Se^{-}), but the values for the selenium and the tin atoms are much smaller because of the strong covalent contributions in the Sn−Se and Se−Se bonds.

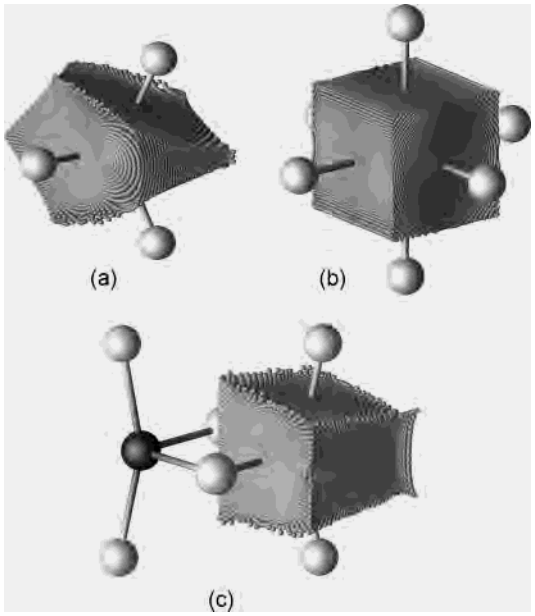

Figure 9. Bader IASs around selected atoms, represented by multitudes of small spheres: (a) Sn2 in the $SnSe_4$ subunits of $Sr_4Sn_2Se_9$, $q(\Omega) = +1.23$; (b) octahedrally coordinated Sn^{2+} in SnSe, $q(\Omega) = +0.84$; (c) Sn1 in Sn_2Se_6 subunits of $Sr_4Sn_2Se_9$, $q(\Omega) = +1.25$.

As the other methods, also the AIM analysis shows clearly that the electronic populations of the two different tin atoms in $Sr_4Sn_2Se_9$ are practically identical, and consequently, we can record the fact that tin in our $Sn_2Se_6^{4-}$ subunits has the chemist's oxidation state 4+. But the different geometry still finds expression in the electronic state of tin. This becomes apparent from the topology of the IAS, i.e., the "shapes" of the tin atoms, which we compare in Figure 9. Figure 9a shows the IAS of tin in the $SnSe_4$ subunit. The topology is rather complex; within its boundaries we integrate a charge of $q_{Sn} = +1.23$. In contrast to this, we show the topology of a true 6-fold-coordinated Sn^{2+} in SnSe with a NaCl-type structure (a high-pressure variant of SnSe). The IAS is of course a cube, but the important point is that the integrated charge is $q_{Sn} = +0.84$, i.e., *much smaller* than for both Sn atoms in our compounds, which have $q_{Sn} = +1.23$ or +1.25.

If we compare the Sn^{4+} ($q_{Sn} \approx +1.24$) and Sn^{2+} ($q_{Sn} = +0.84$) topologies with the corresponding surface around the tin atom in the Sn_2Se_6 subunit in Figure 9c, we find both

differences and similarities. Obviously, this topology resembles a distorted cube similar to that of SnSe in Figure 8b, but the amount of charge therein is almost exactly the same as found in the Sn^{4+} topology of Figure 9a. From this we conclude that there is indeed a distinct difference between the electronic states of tin in the Sn_2Se_6 and $SnSe_4$ subunits of $Sr_4Sn_2Se_9$, but it concerns not the charge nor the oxidation state. Both values are almost equal for both tin atoms, whether we call them atomic charge ($q_{Sn} = +1.24$) or oxidation state (Sn^{4+}). The difference is rather the topology of the atoms, which describes their shape and the volume of space they occupy. Of course, this shape is always a reflection of the environment or coordination of the atom. It describes the deformation of the electron cloud from spherical symmetry that it would have as a free atom. The sum of all interactions such as chemical bonding, crystal packing, etc. generates this unique topology.

Conclusion

The crystal structures of $Sr_4Sn_2Se_9$ and $Sr_4Sn_2Se_{10}$ contain besides the usual $SnSe_4^{4-}$ also $Sn_2Se_6^{4-}$ subunits with unusual large axial Se−Sn−Se angles up to 160.6(1)°. Secondary interactions from two selenium atoms in the equatorial plane of $Sn_2Se_6^{4-}$ are suggestive of a 6-fold octahedral coordination of tin, but long bond distances of 3.36 Å have never been observed in Sn^{4+} selenide chemistry. Next, the AIM analysis shows that the Sn atoms in our $Sn_2Se_6^{4-}$ units are indeed Sn^{4+}, despite their pseudooctahedral coordination. Consequently, we do not consider the long $Sn^{4+}\cdots Se$ interactions to be significant. Also the ELF and COHP analyses do not reveal any definite proof for weak secondary bonding interactions, nor can they give a convincing explanation for the large bond angle in $Sn_2Se_6^{4-}$. All these results together allow only the conclusion that the reason for the unusual geometry comes not out of the $Sn_2Se_6^{4-}$ ion itself and, according to our results, not from secondary interactions. Thus, it does not seem appropriate to treat the covalent $Sn_2Se_6^{4-}$ subunits as if they exist independently, especially not in close-packed solids such as $Sr_4Sn_2Se_9$ and $Sr_4Sn_2Se_{10}$. In our opinion, the special $Sn_2Se_6^{4-}$ geometry is more likely a result of the close packing of the covalent subunits with the strontium ions and the optimization of electrostatic forces between Sr^{2+} and Sn^{4+} cations and $Se^{2-(1-)}$ anions.

Supporting Information Available: X-ray crystallographic information for $Sr_4Sn_2Se_9$ and $Sr_4Sn_2Se_{10}$ in CIF format. This material is available free of charge via the Internet at http://pubs.acs.org.

IC049663Y